Available online at www.sciencedirect.com

ScienceDirect

www.elsevier.com/locate/jes

JES JOURNAL OF ENVIRONMENTAL SCIENCES

www.jesc.ac.cn

Role of glycine on sulfuric acid-ammonia clusters formation: Transporter or participator

Danfeng Li, Dongping Chen, Fengyi Liu, Wenliang Wang *

Key Laboratory for Macromolecular Science of Shaanxi Province, School of Chemistry and Chemical Engineering, Shaanxi Normal University, Xi'an 710119, China

ARTICLE INFO

Article history:
Received 16 July 2019
Received in revised form
7 October 2019
Accepted 23 October 2019
Available online 9 November 2019

Keywords:
New particle formation (NPF)
Glycine
Atmospheric cluster
Atmospheric cluster dynamics code
Enhancement mechanism

ABSTRACT

Glycine (Gly) is ubiquitous in the atmosphere and plays a vital role in new particle formation (NPF). However, the potential mechanism of its on sulfuric acid (SA) - ammonia (A) clusters formation under various atmospheric conditions is still ambiguous. Herein, a $(Gly)_x \cdot (SA)_y \cdot (A)_z$ ($z \leq x + y \leq 3$) multicomponent system was investigated by using density functional theory (DFT) combined with Atmospheric Cluster Dynamics Code (ACDC) at different temperatures and precursor concentrations. The results show that Gly, with one carboxyl (−COOH) and one amine ($-NH_2$) group, can interact strongly with SA and A in two directions through hydrogen bonds or proton transfer. Within the relevant range of atmospheric concentrations, Gly can enhance the formation rate of SA-A-based clusters, especially at low temperature, low [SA], and median [A]. The enhancement (R) of Gly on NPF can be up to 340 at $T = 218.15$ K, $[SA] = 10^4$, $[A] = 10^9$, and $[Gly] = 10^7$ molecules/cm^3. In addition, the main growth paths of clusters show that Gly molecules participate into cluster formation in the initial stage and eventually leave the cluster by evaporation in subsequent cluster growth at low [Gly], it acts as an important "transporter" to connect the smaller and larger cluster. With the increase of [Gly], it acts as a "participator" directly participating in NPF.

Introduction

It has been widely demonstrated that atmospheric aerosols have a widely deleterious effect on air visibility (Huang et al., 2017; Qiao et al., 2018), health of human being (Saikia et al., 2016; Dimitriou and Kassomenos, 2017), and atmospheric circulation directly by changing solar radiation (Baker and Peter, 2008; Deng et al., 2016) and indirectly by serving as cloud condensation nuclei (CNN)/ice nuclei (IN) (Zhang et al., 2012; Meng et al., 2015). New particle formation (NPF) has been observed under various environmental conditions and contributes to more than half of CCN/IN in the atmosphere (Zhang et al., 2015). As the primary source of atmospheric aerosol particles, NPF is generally considered to be a two-step process: First, nucleation forms a "critical nucleus," which then grows to a detectable size (Zhang, 2010). Numerous studies have been investigated the initial formation mechanisms, but there are still many uncertain compositions and the nucleation species that contribute to the formation and growth of atmospheric aerosols particles at the molecular level (Kuang et al., 2011; Kulmala et al., 2013).

* *Corresponding author.*
E-mail address: wlwang@snnu.edu.cn (W. Wang).

https://doi.org/10.1016/j.jes.2019.10.009

Sulfuric acid (SA) is believed to be a common precursor to drive the conversion from gas to particle under various atmospheric conditions (Sipilä et al., 2010), but another component is required to explain observed NPF rates (Kulmala et al., 2004; Weber et al., 2007; Kirkby et al., 2011). Ammonia (A), an important component of increasing atmospheric NPF, is ubiquitous in the atmosphere due to various emission sources ranging from livestock farming to marine organism biodegradation (Schlesinger and Hartley, 1992; Makar et al., 2009; Behera et al., 2013). Noncovalent interaction between SA and A can significantly reduce the partial pressure of SA by forming ammonia sulfate and ammonium bisulfate (Marti et al., 1997). Hence, laboratory and theoretical studies show that A has a greatly influence on the formation rate of SA-based particles (Coffman and Hegg, 1995; Kulmala et al., 2000; Vaittinen et al., 2014). However, even if SA and A are taken into account, the high nucleation rate of aerosols particles in some areas still cannot be well explained under typical atmospheric conditions, which shows that additional precursors species in the atmosphere may be involved in the process of nucleation (Zhang et al., 2012). Nowadays, it has also become clear that more stabilizing species, such as organic nitrogenous compounds (Xie et al., 2017) and highly oxygenated molecules (HOMs) (Elm et al., 2017c; Shi et al., 2019), are more likely to participate in the nucleation of atmospheric NPF within the last decades. Nevertheless, the underlying nucleation mechanism involving organic nitrogen compounds remains unclear.

Organic nitrogen compounds are an important component of atmospheric particulate matter (Mace et al., 2003; Zhang et al., 2002). Approximately 34% of the nitrogen in the atmospheric precipitation exists in the form of organic nitrogen (Cape et al., 2011). The N-containing organic compounds not only serve as CNN/IN but also affect the hygroscopic growth of aerosol particles (Ren et al., 2018). Amino acids are the main component of organic nitrogen compounds, which have been detected in atmospheric aerosols in nearly all geographic regions, ranging from coastal areas to the hinterland (Scalabrin et al., 2012; Ren et al., 2018). In general, sources of amino acids are derived from direct emissions from the terrestrial or marine origin (such as microorganisms and fragments of all varieties of living things), biomass burning, as well as anthropogenic activities (Di Filippo et al., 2014; Ren et al., 2018). It has been proved that organic acids and amines interact strongly with SA, and it obvious enhances the formation rate of SA-containing NPF. The geminate group properties of the amino acids may act as an interesting possibility to participate in NPF (Elm et al., 2013). Many studies have been investigated about the atmospheric roles of amino acids in aerosol particles. For example, Elm et al. (2013) found that glycine (Gly) can be used as a stabilizer of small clusters containing SA in the atmosphere. Wang et al. (2016) pointed out that alanine (Ala) can interact strongly with SA in two directions by hydrogen bonds; the ability to form hydrogen bond is similar to that of A. Ge et al. (2018) indicated that threonine (Thr) may be a possible participant in ion-induced nucleation mainly because Thr·SA isomers have a high value of dipole moment. Similar to Thr, serine (Ser) plays an indispensable role in stabilizing SA and promoting the initial process of NPF. This means that studying clusters of amino acids with atmospheric nucleation precursors is of great importance for gaining a new and insightful understanding of atmospheric nucleation phenomena at the molecular level, especially in the initial stage. Studies indicated that most of the amino acid in PM2.5 are enriched in protein-type glycine (Zhang and Anastasio, 2003). Gly, with one −COOH and $-NH_2$ groups, is the simplest amino acid. Compared with other amino acids, Gly is one of the most abundant amino acids, accounting for 23% of total concentrations of atmospheric amino acids (Barbaro et al., 2011; Scalabrin et al., 2012; Ren et al., 2018). In general, concentrations of glycine range from 10^6–10^9 molecules/cm^3 in the atmosphere (Ren et al., 2018; Zhang and Anastasio, 2003). However, the effect of structural characteristics and thermochemical properties of Gly on the nucleation mechanism of SA and A has almost remained unexplored in NPF.

In this study, we investigated the formation of $(Gly)_x \cdot (SA)_y \cdot (A)_z$ ($z \leq x + y \leq 3$) clusters using density functional theory (DFT) and Atmospheric Cluster Dynamics Code (ACDC) (McGrath et al., 2012) at different temperatures and precursor concentrations with the aims of (1) determining the effect of Gly by comparing formation rates of ternary Gly-SA-A-based cluster with that of binary SA-A-based cluster, (2) exploring the effect of temperature and precursor concentration conditions on the enhancement of Gly, and (3) tracing the influence of Gly on the main growth paths. Overall, this work may lead to a better understanding of the properties of amino acid-containing organic aerosol under typical atmospheric conditions.

1. Computational method

1.1. *Quantum chemical calculations*

All calculations were carried out by using the Gaussian 09 software package (Frisch et al., 2009). Many benchmark studies show that the M06-2X (Zhao and Truhlar, 2008) functional has good performance compared to other common functionals for gaining the Gibbs free energies (Elm et al., 2012; Bork et al., 2014a, 2014b) of atmospheric clusters involving SA. For all the M06-2X calculations the 6–31++G(d,p) basis set was used, as it is a good compromise between accuracy and efficiency and does not yield significant errors in the thermal contribution to the free energy compared to much larger basis sets such as 6–311++G(3df, 3pd) (Elm and Mikkelsen, 2014) and aug-cc-pV5Z4 (Myllys et al., 2016a). So, all optimizations and vibrational frequency were calculated at M06-2X/6–31++G(d, p) level. To identify the lowest Gibbs free energy structure of the organic compounds, firstly the initial structure of 1000 clusters was randomly generated by the ABCluster program (Zhang and Dolg, 2016). All the molecules were described by the CHARMM36 force field (MacKerell et al., 1998) in the ABCluster program. These structures were further optimized by the semiempirical PM6 method (Řezáč et al., 2009) in MOPAC 2016 (Stewart, 2013). Moreover, then, up to 100 conformations with relatively low energies were chosen for re-optimization using M06-2X/6-31 + G(d). Finally, the 10

best of the resulting structures were optimized at the M06-2X/6–31++G(d,p) level of theory. The single-point energy was corrected by a domain-based local pair natural orbital coupled-cluster method DLPNO-CCSD(T) (Riplinger and Neese, 2013) with an aug-cc-pVTZ basis set as implemented in ORCA (Neese, 2012). Recent studies indicated that the DLPNO-CCSD(T)/aug-cc-pVTZ method had been shown to yield a mean absolute error of 0.3 kcal/mol compared to CCSD(T) complete basis set estimates (Elm and Kristensen, 2017b). The configuration optimization, frequency analysis, and the value of $\Delta G_{thermal}$ for relevant clusters were performed at M06-2X/6–31++G(d,p) level. The accurate binding energy (ΔE_{bind}) of corresponding clusters based on the M06-2X geometry was obtained by a higher level of theory (DLPNO-CCSD(T)/aug-cc-pVTZ). The approximate $\Delta G_{bind}^{CCSD(T)}$ value for monomers and clusters was calculated as follows (Myllys et al., 2016b):

$$\Delta G_{bind}^{CCSD(T)} = \Delta E_{bind}^{CCSD(T)} + \Delta G_{thermal}^{DFT}$$

In order to evaluate the effect of temperature on the thermodynamical properties, the Gibbs free energies $\Delta G_{bind}^{CCSD(T)}$ of formation of the clusters were calculated at five different temperatures (218.15, 238.15, 258.15, 278.15, and 298.15 K). The thermochemical parameters are calculated by using a rigid rotor and harmonic oscillator approximations, and all values are reported at 1 atm.

In addition, the ESP analysis was carried out to study reactivity. The topological analysis was performed using Atoms in Molecules (AIM) theory to get insight into the nature of hydrogen bonds (Bader, 1991). The wavefunctions obtained at the M06-2X/6–31++G(d,p) level were used to calculate the electron density ρ and the Laplace electron density $\nabla^2\rho$ at the bond critical points (BCPs). All wavefunction analysis was performed by Multiwfn 3.6 package (Lu and Chen, 2012).

1.2. *Atmospheric Cluster Dynamics Code (ACDC) kinetic model*

The ACDC is a dynamical program to model the kinetics of clusters by an explicit solution of the birth-death equation (McGrath et al., 2012) using the ode15s solver in the MATLAB-R2014a program (Shampine and Reichelt, 1997), which is effective in solving systems of stiff differential equations. The birth-death equation can be written as (McGrath et al., 2012)

$$\frac{dc_i}{dt} = \frac{1}{2}\sum_{j<i}\beta_{j,(i-j)}c_j c_{(i-j)} + \sum_j \gamma_{(i+j)\to i}c_{(i+j)} - \sum_j \beta_{i,j}c_i c_j - \frac{1}{2}\sum_{j<i}\gamma_{i\to j}c_i + Q_i - S_i$$

where, c_i and c_j are the concentration of the clusters i and j, $\beta_{i,j}$ is the collision coefficient between clusters i and j, $\gamma_{i\to j}$ is the evaporation coefficient of cluster i into cluster j, Q_i and S_i are possible additional source and sink terms of cluster i, respectively. A coagulation sink coefficient of 2.6×10^{-3} s^{-1} was used for all clusters (Dal Maso et al., 2008; Zhang et al., 2017), as it is the median condensation sink coefficient of sulfuric acid vapor on pre-existing aerosol particles. Variations in this value between 10^{-3} s^{-1} and 5×10^{-3} s^{-1} did not affect the main conclusions of this kind of study (Bork et al., 2014a, 2014b).

For clusters i and j the collision rate coefficient $\beta_{i,j}$ was given as (Steinfeld, 2006)

$$\beta_{i,j} = \pi(r_i + r_j)^2\sqrt{\frac{8k_BT}{\pi\mu}}$$

where, r_i and r_j are the radius of cluster i and j, k_B is the Boltzmann constant, T is the temperature, and $\mu = m_i m_j/(m_i + m_j)$ is the reduced mass of cluster i and j. The cluster radius is half of the sum of the distance between the center of the most distant atoms in the cluster given by the Multiwfn 3.6 program (Lu and Chen, 2012) and the van der Waals radii of these atoms.

Evaporation coefficients $\gamma_{(i+j)\to i}$ can be calculated from the corresponding collision coefficients and the Gibbs free energies of formation of clusters using (McGrath et al., 2012)

$$\gamma_{(i+j)\to i} = \beta_{i,j}\frac{p_{ref}}{k_BT}\exp\left(\frac{\Delta G_{i+j} - \Delta G_i - \Delta G_j}{k_BT}\right)$$

where ΔG is the quantum mechanically calculated free energy at the reference pressure p_{ref} (in this case, 1 atm). For the reaction of monomer molecules i and j to form cluster $(i + j)$, the Gibbs free energy of formation of the cluster $(i + j)$ is

$$\Delta G_{i+j} = G_{i+j} - (\Delta G_i + \Delta G_j)$$

In this paper, water molecules were not considered because of the large computational costs required to obtain the necessary thermodynamic data of the hydrated clusters. Generally, hydration can be expected to stabilize weakly bound clusters more than strongly bound clusters (Bork et al., 2014a, 2014b). For the studied system, the interactions between acid and base molecules are stronger than those hydrogen bonds, and hydration is not likely to have a significant effect on the stability of clusters. Thus the main growth pathways are not expected to be affected significantly by hydration (Paasonen et al., 2012; Almeida et al., 2013; Henschel et al., 2014).

In addition, the maximum total number of acid and base molecules is 3. The flux outside of the system studied for a cluster is determined by choice of boundary conditions. The boundary conditions require the outgrowing clusters to have a favorable composition so that the clusters are stable enough not to evaporate back immediately. In general, when the number of acid molecules is equal to or more than that of base molecules, these clusters have the potential to further grow into larger sizes (Paasonen et al., 2012), a neutral cluster or a weakly acidic cluster is more favorable for the subsequent cluster growth. Considering the formation Gibbs free energy (Appendix A Table S2) and evaporation rates (Appendix A Table S1) of all clusters, it can be found that the clusters containing pure SA and A molecules as well as the clusters containing a Gly molecule are mostly more stable and therefore are allowed to form larger clusters and contribute to particle formation rates. In this case, clusters $(SA)_4\cdot(A)_2$ and $Gly\cdot(SA)_3\cdot(A)_2$ are set to be boundary clusters.

2. Results and discussion

2.1. Structures and thermodynamics

There are altogether 27 most stable structures in $(Gly)_x \cdot (SA)_y \cdot (A)_z$ ($z \leq x + y \leq 3$) system obtained at M06-2X/6–31++G(d,p) level. Eight key hydrogen-bonded cluster structures with the lowest Gibbs free energy are presented in Fig. 1. The $\Delta G_{bind}^{CCSD(T)}$ of corresponding clusters are shown in Table 1. Structures and thermodynamic properties for all other clusters are listed in Appendix A. The –COOH and $-NH_2$ groups in Gly directly combine with SA and A by hydrogen bonds in all clusters. This indicates that glycine can form hydrogen bonds in two directions to enhance the formation rate and further stabilize small clusters. The relative stabilities of clusters could be assessed by

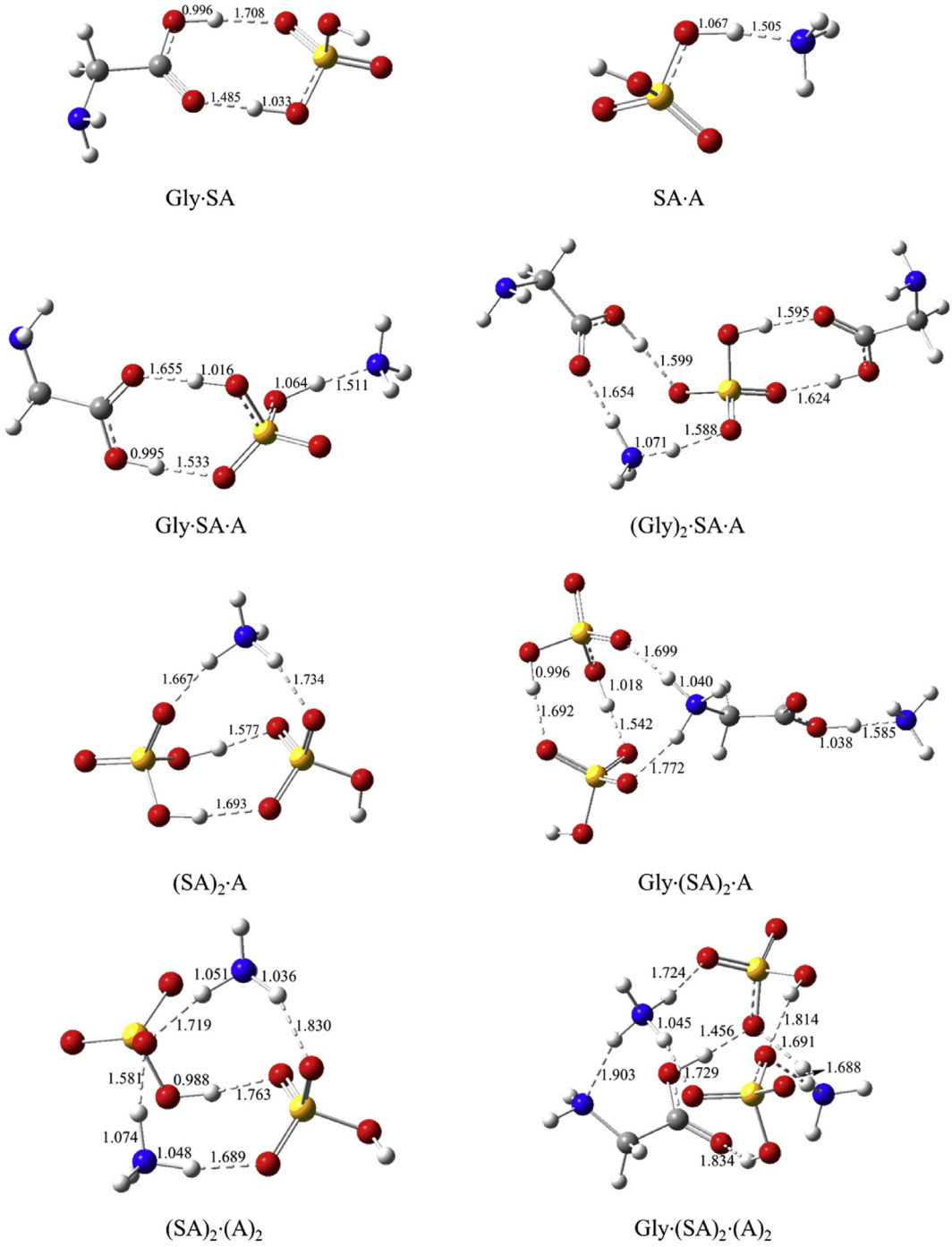

Fig. 1 – The molecular structures of the identified lowest Gibbs free energy complexes at the M06-2X/6–31++G(d,p) level of theory. The distances are given in angstroms. The red balls represent oxygen atoms, blue is for nitrogen atoms, yellow is for sulphur atoms, and white is for hydrogen atoms.

Table 1 – Reaction Gibbs free energies of formation ($\Delta G_{bind}^{CCSD(T)}$) for clusters composed of atmospheric precursors calculated at 298.15 K and 1 atm. (kcal/mol).

Reactions	$\Delta G_{bind}^{CCSD(T)}$
Gly + SA → Gly·SA	−9.30
Gly + A → Gly·A	−5.58
SA + A → SA·A	−8.34
Gly + SA + A → Gly·SA·A	−17.69
$(Gly)_2$ + SA + A → $(Gly)_2$·SA·A	−26.11
$(SA)_2$ + A → $(SA)_2$ A	−27.14
Gly + $(SA)_2$ + NH_3 → Gly·$(SA)_2$ A	−34.82
$(SA)_2$ + $(A)_2$ → $(SA)_2$·$(A)_2$	−36.19
Gly + $(SA)_2$ + $(A)_2$ → Gly·$(SA)_2$·$(A)_2$	−44.77

Gly: glycine; SA: sulfuric acid; A: ammonia.

comparing their formation energies in NPF process (Ge et al., 2018). As can be seen in Fig. 1, the values of $\Delta G_{bind}^{CCSD(T)}$ both Gly·SA and SA·A cluster are −9.30 and −8.34 kcal/mol, respectively. It indicates that Gly·SA cluster is more stable than SA·A cluster. For Gly·SA studied here, one cycle structure is formed by two intermolecular hydrogen bonds. Proton transfer did not occur, but the length of OH covalent bond in Gly·SA cluster increased by 0.026 Å compared original length of OH bond (0.970 Å) in Gly monomer. These characteristics differ from the case of Thr·SA and Ser·SA clusters, where one proton is transferred from SA to Thr and Ser due to the effect of the substituent group (Ge et al., 2018). These results suggest that different amino acids have different interaction patterns with sulfuric acid. This further indicates that Gly may play an extremely important role in stabilizing and promoting initial formation processes of SA-containing NPF.

When one Gly molecule was added to SA·A cluster to form Gly·SA·A cluster, SA directly binds with A and one proton is transferred from SA to A, but Gly only binds with SA through hydrogen bonding and the proton transfer did not occur. The previous studies (Liu et al., 2018; Zhang et al., 2018a, 2018b) suggest that the formation path has changed significantly in these clusters containing at least two Gly molecules. These clusters containing two Gly molecules are a primary focus later. It is noted that an intermolecular proton transfer occurred when the second Gly molecular was added to the Gly·SA·A cluster. In the $(Gly)_2$·SA·A cluster, one proton is transferred from SA to A to form $-NH_3^+$ ion, meanwhile, the length of OH bond in SA is elongated by 0.572 Å. Another proton is transferred from SA to the N atom in Gly to form $[Gly-H]^+$ ion structure. The values of $\Delta G_{bind}^{CCSD(T)}$both Gly·SA·A and $(Gly)_2$·SA·A are −17.69 and −26.11 kcal/mol, respectively. It indicates that the formation of Gly·SA·A and $(Gly)_2$·SA·A clusters are spontaneous process from a thermodynamic point of view. It is obvious that more glycine molecules are favorable for the stable SA-A-based cluster. In addition, the values of $\Delta G_{bind}^{CCSD(T)}$ both Gly·$(SA)_2$ A and Gly·$(SA)_2$·$(A)_2$ decreased by 7.68 and 8.58 kcal/mol compared that of $(SA)_2$ A (−27.14 kcal/mol) and $(SA)_2$·$(A)_2$ (−36.19 kcal/mol), respectively. It also suggests that the presence of Gly is beneficial to the formation of SA-A-based cluster. However, in larger clusters, SA is significantly more stabilized compared to Gly, which is mainly due to its strong acidity. Additionally, besides the Gly dimer, clusters containing more than one Gly molecule are less stable than corresponding SA-containing analogues (Appendix A Table S2). When the total number of A molecules is equal to or less than the total number of acid (Gly and SA) molecules, A molecule is protonated easily. One proton is transferred from SA to A molecule, but the SO_4^{2-} ion is not found in all clusters because the complete deprotonating of SA hardly occurs in actual atmospheric environments.

For studying and predicting intermolecular interaction sites between Gly with SA and A molecules, an in-depth investigation of the ESP on molecular vdW surface is further studied (Lu and Manzetti, 2014). In the process of clustering, the binding site could be analyzed by combing the featured group and ESP. The site possessing more negative ESP has a stronger ability to attract proton while those with more positive ESP tend to provide proton if the proton is available (Manzetti and Lu, 2013). Here we take the Gly·$(SA)_2$ A cluster, for instance, since both −COOH and $-NH_2$ are directly involved in nucleation among ternary Gly-involved cluster. As can be seen in Fig. 2, all molecules have some electropositive extreme points (little cyan spheres) and electronegative extreme points (little yellow spheres) on the molecular vdW surface, which means that all molecules can be used as either donor or acceptor. The electropositive extreme points are on N and O atoms, and the electronegative extreme points are on H atoms, especially which connected to N or O atoms. It is found that hydrogen bond interaction mainly occurs at the extreme points between electropositive and electronegative. Finally, hydrogen bonds form to make the cluster energy as low as possible.

In order to investigate the interaction strength in all clusters formed by nucleation precursors, the electron density ρ and the Laplace electron density $\nabla^2\rho$ at the BCPs were analyzed by AIM at M06-2X/6–31++G(d,p) level, are listed in Appendix A Table S3. A positive value of $\nabla^2\rho$ at the BCPs suggests the closed-shell interactions, whereas the value of $\nabla^2\rho$ for covalent bond is negative. The strength of the hydrogen bonds correlates with ρ (Gilli et al., 1994; Zhang et al., 2018a, 2018b). Two quantitative criteria have been suggested to characterize the types of hydrogen bond: ρ and $\nabla^2\rho$, in the range of 0.002–0.035 and 0.024–0.139 a.u., respectively (Grabowski, 2004; Koch and Popelier, 1995). For those clusters studied, the electron densities ρ at the BCPs are in the range of 0.013–0.086 a.u. and the Laplace electron densities $\nabla^2\rho$(BCPs) ranges from 0.047 a.u. to 0.181 a.u.. These values are higher than the upper value of the criteria for a hydrogen bond due to the strong hydrogen bonding induced by the acid-base reaction. The topological analysis indicates that strong hydrogen bonding exists extensively in clusters studied.

2.2. *Clustering enhancements*

To analyze the clustering abilities of Gly, a series of ACDC simulations based on these thermodynamics were performed under different conditions. A suitable measure for the enhancement of the cluster formation rates is the ratio (R) in the existence of Gly to that without Gly,

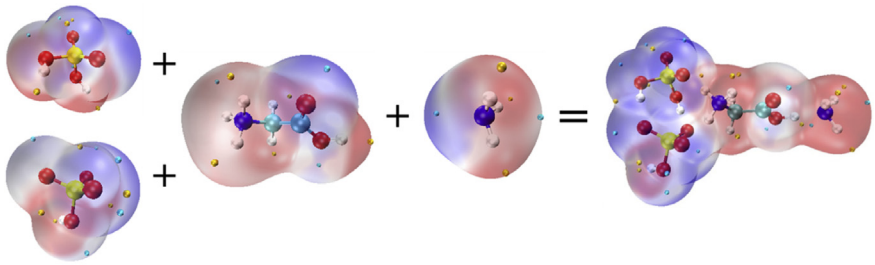

Fig. 2 – The Electrostatic Potential (ESP) analysis of SA, Gly, A and Gly·$(SA)_2$ A cluster. The red, yellow, blue, cyan and white balls stand for O, S, N, C and H atoms, respectively. Small yellow and cyan spheres on the surface of molecular van der Waals are represented max-positive and mini-negative locations of ESP, respectively.

$$R=\frac{J([SA]=a,[A]=b,[Gly]=c)}{J([SA]=a,[A]=b,[Gly]=0)}$$

where J denotes the cluster formation rate under the indicated conditions and a, b, c stands for the monomer concentrations of SA, A, and Gly. The concentrations of SA, A are set to be 10^4–10^8 and 10^7–10^{11} molecules/cm^3, which are related to the corresponding atmospheric concentration (Riipinen et al., 2007; Benson et al., 2011; Almeida et al., 2013; Schobesberger et al., 2013). The Gly concentration is set to be 10^6–10^9 molecules/cm^3, which is in the range of its detected atmospheric concentrations (Ren et al., 2018). When R is larger than 1.0, Gly will show the enhancement effect of SA-A-based clusters. The generated R at varying temperatures ranging from 218.15 to 258.15 K and different concentrations are summarized in Appendix A Tables S4–S6.

2.2.1. *The influence of temperature on* R

Fig. 3 shows the effect of temperature on R of Gly at varying SA and A concentrations under the conditions of [Gly] = 10^7 molecules/cm^3 in the system. The red, green and blue lines represent the low, median and high concentrations of SA, respectively. The square, circle and triangle lines represent the low, median and high concentrations of A, respectively.

From Fig. 3, the common trend is that the enhancement of Gly on the formation rate of clusters decreases gradually with the increase of temperature in all simulation ranges. The value of R begins to be obvious at the temperature of lower than 238.15 K. The R reaches the highest value at low SA concentration (10^4 molecules/cm^3) and median A concentration (10^7 molecules/cm^3) and can be as high as 340 at 218.15 K. The value of R moderately decreased with the increase of temperature at 238.15 K $\leq T \leq$ 278.15 K, and it approximately equals 1.0 when $T >$ 278.15 K. The main reason is that the Gibbs free energies of the clusters increase with the increase of temperature, and the evaporation rate of monomer increases correspondingly, which ultimately leads to the decrease of the cluster formation rate. Hence, the temperature 218.15 K will be a proper choice for the further research. At different Gly concentrations, the variation of R is approximately the same (Appendix A Fig. S1).

2.2.2. *Influence of concentration on* R

In order to understand the relationship among the monomers, the effect of concentration on R of Gly was further studied. Fig. 4 shows the R under the different concentration conditions. It is observed that R increases gradually with the increase of [Gly].

Fig. 4a shows that the value of R decreases with the increase of [SA], and the change of R is the most obvious at low [SA]. This is mainly because the acidity of SA is stronger than that of Gly, SA·A cluster (−10.81 kcal/mol) is more stable than the Gly·A cluster (−7.92 kcal/mol) (Appendix A Table S2), leads to a competition between SA and Gly in the process of interaction with A. When the [A] and [Gly] is changeless, the added SA molecule can bind with A, causing the initial Gly·A hydrogen bonds to break and the new SA·A hydrogen bonds to form. In addition, the evaporation rate of Gly·A cluster is higher than those of SA·A cluster (Appendix A Table S1). Finally, R decreases even if the overall particle rate increases.

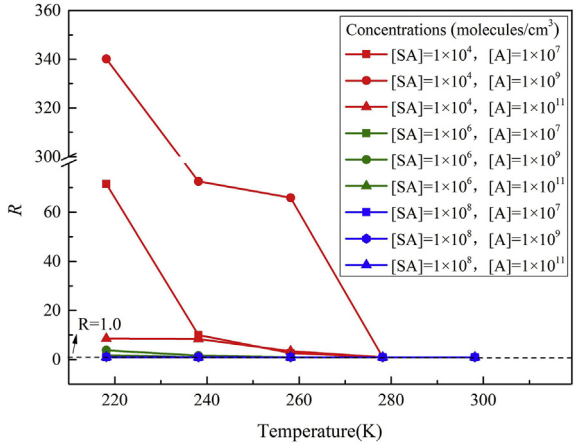

Fig. 3 – The enhancement (R) of Gly on the formation rate of clusters at varying temperatures ranging from 218.15 to 298.15 K and varying concentrations of SA and A. All the simulations were under the conditions of [Gly] = 10^7 molecules/cm^3.

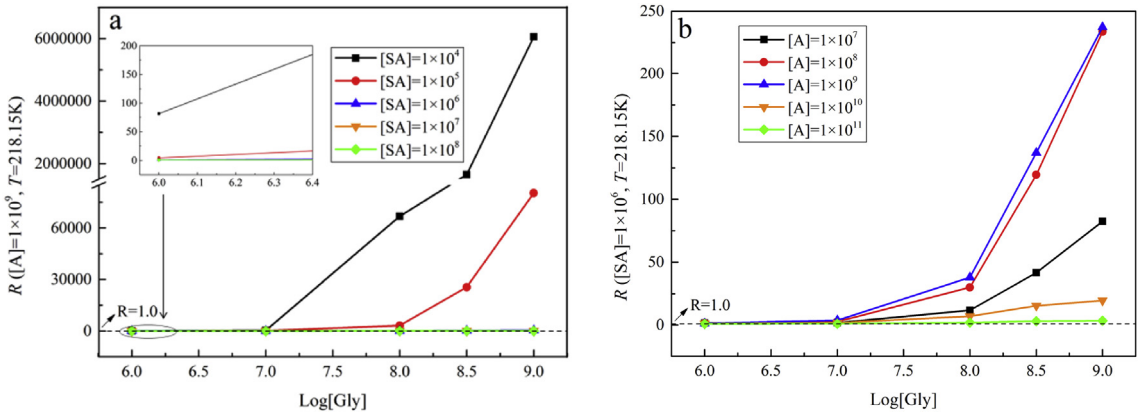

Fig. 4 – The enhancement (*R*) of Gly on the formation rate of clusters at varying [Gly] ranging from 10^6 to 10^9 molecules/cm^3. All the simulations were under the conditions of $T = 218.15$ K. (a) [A] = 10^9 molecules/cm^3; (b) [SA] = 10^6 molecules/cm^3.

From Fig. 4b, it is found that the effect of [A] on *R* is completely different from [SA]. *R* firstly increases and then decreases with the increase of [A]. *R* can reach the maximum value of 240 at [A] = 10^9 molecules/cm^3. This phenomenon may be explained by intermolecular interactions. As the only base molecule existed in the system studied, the increased number of A molecule can provide more hydrogen bonding sites for the Gly and SA. *R* firstly increases when [A] is low, there may be additional Gly molecules that have not been fully bonded. Therefore, Gly shows an enhancement effect by interacting with A through hydrogen bonds. With the increase of [A], Gly can approach to interaction sites saturation, thus reaching the maximum enhancement of Gly. Subsequently the added A molecules will break the hydrogen bonds between Gly and SA, leading to the decreased interaction between Gly and SA molecules, and making the interaction sites of Gly unsaturated, thereby decreasing *R*. The same conclusion can be obtained at varying concentration conditions in Appendix A Figs. S2-S3.

2.3. *Growth paths*

In order to further determine the enhancement mechanism of Gly, the main growth paths of the cluster were traced by ACDC. According to section 2.2, *R* reaches the maximum value at this condition where $T = 218.15$ K, [SA] = 10^4, [A] = 10^9 molecules/cm^3. Hence, the following researches were performed at the same conditions. Growth paths of Gly-SA-A-based clusters at three different Gly concentrations (10^6, 10^7, and 10^8 molecules/cm^3) are presented in Fig. 5. The green and red lines represent the growth paths of pure SA-A-based clusters and Gly-containing cluster, respectively.

As can be seen in Fig. 5, the growth paths of pure SA-A-based clusters are the same, but the growth paths of Gly-containing cluster are significantly different. From the green line, the formation of $(SA)_2$ and SA·A is the first step. Secondly, the $(SA)_2$ A cluster is formed by the collision of $(SA)_2$ and A, and SA·A and SA. Then, $(SA)_2$ A collides with A molecular to form $(SA)_2\cdot(A)_2$ cluster, and it collides with SA molecular to form $(SA)_3\cdot(A)_2$ cluster. Finally, as a primary cluster of flux out, the $(SA)_3\cdot(A)_2$ cluster grows out of the simulated system. The growth paths of SA-A-based clusters are inconsistent with those previous studies (Li et al., 2018a, 2018b). For different red line, the growth mechanism of Gly-containing clusters is simple at low [Gly]. With the increase of [Gly], the growth mechanism becomes more complicated. When [Gly] = 10^6 molecules/cm^3 (Fig. 5a), Gly·SA·A and $(Gly)_2$·SA·A, as the initially generated Gly-containing clusters, are formed by the collision of one and two Gly molecules with SA·A cluster, respectively. From Section 2.1, the $(Gly)_2$·SA·A cluster is more stable than Gly·SA·A cluster, and the former has a higher evaporation rate (4.92×10^{-2} s^{-1}) and is easily converted to Gly·SA·A cluster by evaporation of Gly monomer (Appendix A Table S1). After it, Gly·SA·A cluster collides with SA·A to form Gly·$(SA)_2$·$(A)_2$ cluster. However, it is found that the main flux out is the $(SA)_2$·$(A)_2$ cluster rather than Gly·$(SA)_2$·$(A)_2$ cluster, it is confirmed that Gly molecule plays a role of "transporter" in clusters growth at low [Gly]. When [Gly] is increased to 10^7 molecules/cm^3 (Fig. 5b), it is found that there is an additional growth path originated from the collision of one Gly and one SA molecule formed Gly·SA cluster in the initial stage of clusters formation. The growth path of containing Gly molecules is different from those paths in Fig. 5a, the main reason is that the Gly·SA dimer ($\Delta G_{bind}^{CCSD(T)} = -12.14$ kcal/mol) is very stable in the whole system (Appendix A Table S2). The previous study (Elm, 2017a; Liu et al., 2018; Li et al., 2018b) shows that the stability of acid-base clusters is far higher than that of pure acid clusters due to more hydrogen bonds and strong electrostatic interaction, namely "base stabilization mechanism." After, the collision of Gly·SA with A formed Gly·SA·A cluster via a similar base stabilization mechanism, the Gly·SA·A cluster grows through the following two paths: (1) Gly·SA·A → Gly·$(SA)_2$ A → Gly·$(SA)_2$·$(A)_2$ (41%)→ flux out and (2) Gly·SA·A → Gly·$(SA)_2$·$(A)_2$ (17%) → flux out. It is obvious that Gly·$(SA)_2$ A cluster is a very important intermediate due to its strong hydrogen bonding, low $\Delta G_{bind}^{CCSD(T)}$, and low evaporation rate. It also suggests that the path (2) is favorable for the subsequent growth of clusters. The Gly molecule shows an ability to directly participate in the cluster formation, suggesting that the role of Gly is a "participator" in the nucleation process. When [Gly] = 10^8 molecules/cm^3 (Fig. 5c), it is found that the number of growth paths containing Gly molecules continuously increase. The enhancement strength *R* gradually

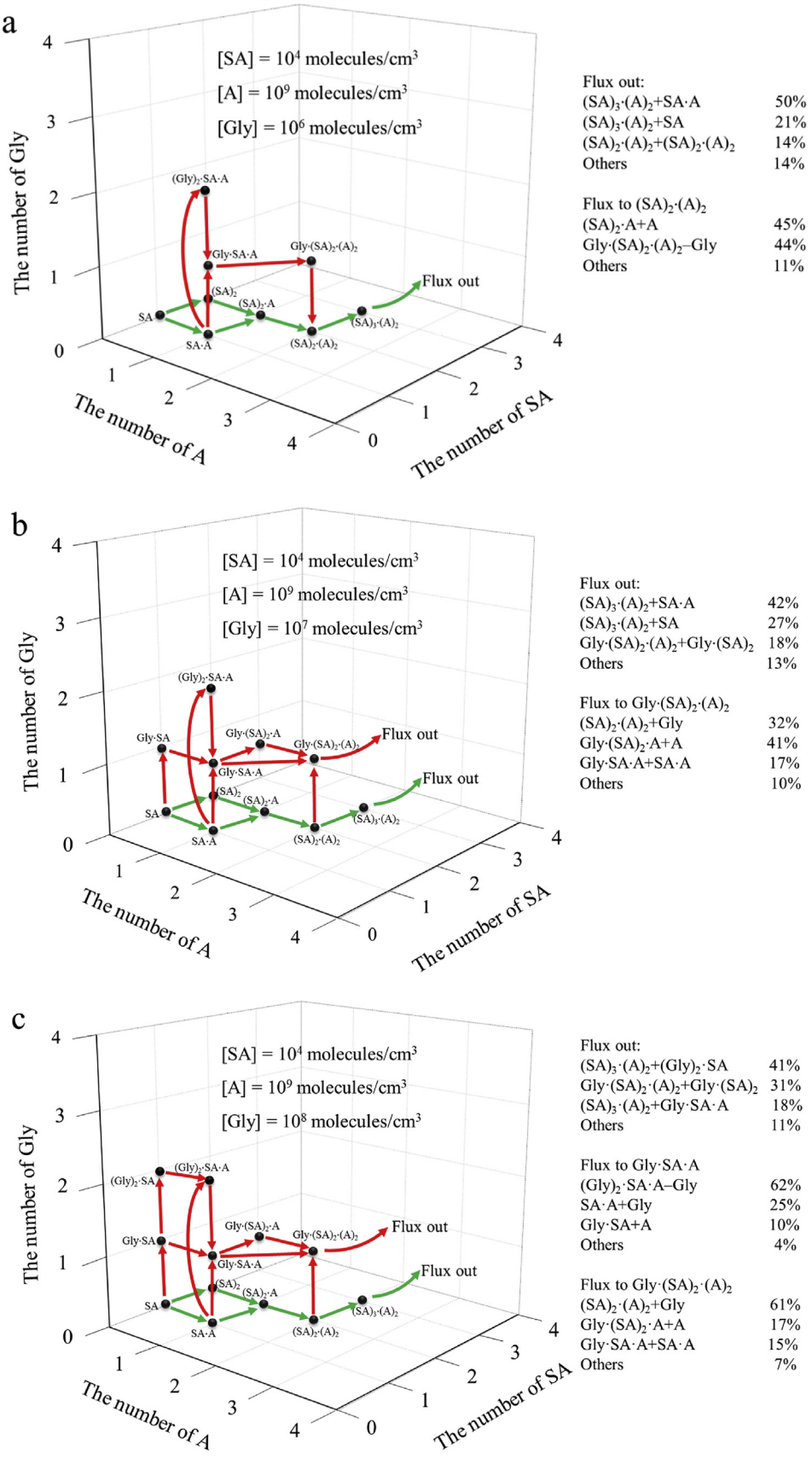

Fig. 5 – Main growth paths of the simulated system at $T = 218.15$ K with varying [Gly]. (a) 10^6 molecules/cm^3; (b) 10^7 molecules/cm^3; (c) 10^8 molecules/cm^3. The green and red flux stands for the paths containing pure SA-A-based clusters and Gly molecules, respectively.

increases with the increase of [Gly], which further confirmed that the role of Gly in the formation of clusters is more and more important. The formation of Gly·SA·A cluster follows the following three growth paths: (1) SA·A → Gly·SA·A (25%) (2) $(Gly)_2$·SA·A → Gly·SA·A (62%) (3) Gly·SA → Gly·SA·A (10%). The main growth path is path (2), which is formed $(Gly)_2$·SA·A cluster and eventually evaporate a Gly molecule. Subsequently, the Gly·SA·A cluster grows to form Gly·$(SA)_2$·$(A)_2$ cluster. Finally the Gly·$(SA)_2$·$(A)_2$ cluster grows out of the system. The Gly molecule plays the part of "participator" in NPF. This shows that with the further increase of [Gly], its role becomes even more important. Though the concentration of glycine is not high in some areas, it can cycle to use in facilitating NPF.

3. Conclusions

Glycine is abundant in the gas and aerosol phases (Barbaro et al., 2011; Ren et al., 2018; Scalabrin et al., 2012; Zhang and Anastasio, 2003). The role of Gly in the formation of molecular clusters in atmospheres containing various quantities of Gly, SA and A are studied using the ACDC kinetic model and DFT calculations. The main conclusions are summarized as follows:

(a) Gly has two functional groups (−COOH and $-NH_2$) that can enhance the formation of small clusters through hydrogen bonds or proton transfer in two directions.
(b) The enhancement *R* presents a positive dependence on [Gly] and a negative dependence on temperatures. The enhancement *R* of Gly decreases with the increase of [SA]. Moreover, *R* firstly increases and then decreases with the increase of [A].
(c) The Gly-containing clusters can directly participate in the cluster formation and eventually leave the cluster by evaporation at low [Gly]. The role of Gly can be a "transporter" to connect the smaller and larger clusters. With the increase of [Gly], it could directly participate in the growth path and act as a "participator" in NPF.

Acknowledgments

This work was supported by the National Natural Science Foundation of China (Nos: 21473108, 21873060, 21636006) and The Fundamental Research Funds for the Central Universities (No. GK201901007). Furthermore, we gratefully acknowledge the valuable help of Prof. Hanna Vehkamäki (University of Helsinki), Prof. Tinja Olenius (Stockholm University), and Prof. Xiuhui Zhang (Beijing Institute of Technology).

Appendix A. Supplementary data

Supplementary data to this article can be found online at https://doi.org/10.1016/j.jes.2019.10.009.

REFERENCES

Almeida, J., Schobesberger, S., Kürten, A., Ortega, I.K., Kupiainen-Määttä, O., Praplan, A.P., et al., 2013. Molecular understanding of sulphuric acid-amine particle nucleation in the atmosphere. Nature 502, 359–365.
Bader, R.W., 1991. A quantum theory of molecular structure and its applications. Chem. Rev. 91, 893–928.
Baker, M.B., Peter, T., 2008. Small-scale cloud processes and climate. Nature 451, 299–300.
Barbaro, E., Zangrando, R., Moret, I., Barbante, C., Cescon, P., Gambaro, A., 2011. Free amino acids in atmospheric particulate matter of Venice. Italy. Atmos. Enviro. 45, 5050–5057.
Behera, S.N., Sharma, M., Aneja, V.P., Balasubramanian, R., 2013. Ammonia in the atmosphere: a review on emission sources, atmospheric chemistry and deposition on terrestrial bodies. Environ. Sci. Pollut. Res. 20, 8092–8131.
Benson, D.R., Yu, J.H., Markovich, A., Lee, S.H., 2011. Ternary homogeneous nucleation of H_2SO_4, NH_3, and H_2O under conditions relevant to the lower troposphere. Atmos. Chem. Phys. 11, 4755–4766.
Bork, N., Du, L., Kjaergaard, H.G., 2014a. Identification and characterization of the HCl-DMS gas phase molecular complex via infrared spectroscopy and electronic structure calculations. J. Phys. Chem. A 118, 1384–1389.
Bork, N., Elm, J., Olenius, T., Vehkamäki, H., 2014b. Methane sulfonic acid-enhanced formation of molecular clusters of sulfuric acid and dimethyl amine. Atmo. Chem. Phys. 14, 12023–12030.
Cape, J.N., Cornell, S.E., Jickells, T.D., Nemitz, E., 2011. Organic nitrogen in the atmosphere — Where does it come from? A review of sources and methods. Atmos. Res. 102, 30–48.
Coffman, D.J., Hegg, D.A., 1995. A preliminary study of the effect of ammonia on particle nucleation in the marine boundary layer. J. Geophys. Res.-Atmos. 100, 7147–7160.
Dal Maso, M., Hyvärinen, A., Komppula, M., Tunved, P., Kerminen, V., Lihavainen, H., et al., 2008. Annual and interannual variation in boreal forest aerosol particle number and volume concentration and their connection to particle formation. Tellus B 60, 495–508.
Deng, X.L., Shi, C.E., Wu, B.W., Yang, Y.J., Jin, Q., Wang, H.L., et al., 2016. Characteristics of the water-soluble components of aerosol particles in Hefei, China. J. Environ. Sci. 42, 32–40.
Di Filippo, P., Pomata, D., Riccardi, C., Buiarelli, F., Gallo, V., Quaranta, A., 2014. Free and combined amino acids in size-segregated atmospheric aerosol samples. Atmos. Environ. 98, 179–189.
Dimitriou, K., Kassomenos, P., 2017. Airborne heavy metals in two cities of North Rhine Westphalia-performing inhalation cancer risk assessment in terms of atmospheric circulation. Chemosphere 186, 78–87.
Elm, J., 2017a. Elucidating the limiting steps in sulfuric acid-base new particle formation. J. Phys. Chem. A 121, 8288–8295.
Elm, J., Kristensen, K., 2017b. Basis set convergence of the binding energies of strongly hydrogen-bonded atmospheric clusters. Phys. Chem. Chem. Phys. 19, 1122–1133.
Elm, J., Mikkelsen, K.V., 2014. Computational approaches for efficiently modelling of small atmospheric clusters. Chem. Phys. Lett. 615, 26–29.
Elm, J., Bilde, M., Mikkelsen, K.V., 2012. Assessment of density functional theory in predicting structures and free energies of reaction of atmospheric prenucleation clusters. J. Chem. Theory Comput. 8, 2071–2077.

Elm, J., Fard, M., Bilde, M., Mikkelsen, K.V., 2013. Interaction of glycine with common atmospheric nucleation precursors. J. Phys. Chem. A 117, 12990–12997.
Elm, J., Myllys, N., Kurtén, T., 2017c. What is required for highly oxidized molecules to form clusters with sulfuric acid? J. Phys. Chem. A 121, 4578–4587.
Frisch, M.J., Trucks, G.W., Schlegel, H.B., Scuseria, G.E., Robb, M.A., Cheeseman, J.R., et al., 2009. Gaussian 09, Revision D.01. Gaussian, Inc., Wallingford, CT.
Ge, P., Luo, G., Luo, Y., Huang, W., Xie, H.B., Chen, J.W., Qu, J.P., 2018. Molecular understanding of the interaction of amino acids with sulfuric acid in the presence of water and the atmospheric implication. Chemosphere 210, 215–223.
Gilli, P., Bertolasi, V., Ferretti, V., Gilli, G., 1994. Covalent nature of the strong homonuclear hydrogen bond. Study of the O-H-O system by crystal structure correlation methods. J. Am. Chem. Soc. 116, 909–915.
Grabowski, S.J., 2004. Hydrogen bonding strength-measures based on geometric and topological parameters. J. Phys. Org. Chem. 17, 18–31.
Henschel, H., Navarro, J.C., Yli-Juuti, T., Kupiainen-Määttä, O., Olenius, T., Ortega, I.K., et al., 2014. Hydration of atmospherically relevant molecular clusters: computational chemistry and classical thermodynamics. J. Phys. Chem. A 118, 2599–2611.
Huang, X.F., Wang, C., Peng, J.F., He, L.Y., Cao, L.M., Zhu, Q., et al., 2017. Characterization of particle number size distribution and new particle formation in Southern China. J. Environ. Sci. 51, 342–351.
Kirkby, J., Curtius, J., Almeida, J., Dunne, E., Duplissy, J., Ehrhart, S., et al., 2011. Role of sulphuric acid, ammonia and galactic cosmic rays in atmospheric aerosol nucleation. Nature 476, 429–433.
Koch, U., Popelier, P.L.A., 1995. Characterization of C-H-O Hydrogen Bonds on the Basis of the Charge Density. J. Phys. Chem. 99, 9747–9754.
Kuang, C., Chen, M., Zhao, J., Smith, J.,, McMurry, P.H., Wang, J., 2011. First size-dependent growth rate measurements of 1 to 5 nm freshly formed atmospheric nuclei. Atmos. Chem. Phys. 11, 25427–25471.
Kulmala, M., Pirjola, L., Makela, J.M., 2000. Stable sulphate clusters as a source of new atmospheric particles. Nature 404, 66–69.
Kulmala, M., Vehkamäki, H., Petäjä, T., Dal Maso, M., Lauri, A., Kerminen, V.M., et al., 2004. Formation and growth rates of ultrafine atmospheric particles: a review of observations. J. Aerosol Sci. 35, 143–176.
Kulmala, M., Kontkanen, J., Junninen, H., Lehtipalo, K., Manninen, H.E., Nieminen, T., et al., 2013. Direct observations of atmospheric aerosol nucleation. Science 339, 943–946.
Li, H., Zhang, X.H., Zhong, J., Liu, L., Zhang, H.J., Chen, F., et al., 2018a. The role of hydroxymethanesulfonic acid in the initial stage of new particle formation. Atmo. Environ. 189, 244–251.
Li, H., Zhong, J., Vehkamäki, H., Kurtén, T., Wang, W.G., Ge, M.F., et al., 2018b. Self-catalytic reaction of SO_3 and NH_3 to produce sulfamic acid and its implication to atmospheric particle formation. J. Am. Chem. Soc. 140, 11020–11028.
Liu, L., Li, H., Zhang, H.J., Zhong, J., Bai, Y., Ge, M.F., et al., 2018. The role of nitric acid in atmospheric new particle formation. Phys. Chem. Chem. Phys. 20, 17406–17414.
Lu, T., Chen, F., 2012. Multiwfn: a multifunctional wavefunction analyzer. J. Comput. Chem. 33, 580–592.
Lu, T., Manzetti, S., 2014. Wavefunction and reactivity study of benzo[a]pyrene diol epoxide and its enantiomeric forms. Struct. Chem. 25, 1521–1533.
Mace, K.A., Kubilay, N., Duce, R.A., 2003. Organic nitrogen in rain and aerosol in the eastern mediterranean atmosphere: an association with atmospheric dust. J. Geophys. Res.-Atmos. 108, 4320.
MacKerell, A.D., Bashford, D., Bellott, M., Dunbrack, R.L., Evanseck, J.D., Field, M.J., et al., 1998. All-atom empirical potential for molecular modeling and dynamics studies of proteins. J. Phys. Chem. B 102, 3586–3616.
Makar, P.A., Moran, M.D., Zheng, Q., Cousineau, S., Sassi, M., Duhamel, A., et al., 2009. Modelling the impacts of ammonia emissions reductions on North American air quality. Atmos. Chem. Phys. 9, 7183–7212.
Manzetti, S., Lu, T., 2013. The geometry and electronic structure of aristolochic acid: possible implications for a frozen resonance. J. Phys. Org. Chem. 26, 473–483.
Marti, J.J., Jefferson, A., Cai, X.P., Richert, C., McMurry, P.H., Eisele, F., 1997. H_2SO_4 vapor pressure of sulfuric acid and ammonium sulfate solutions. J. Geophys. Res.-Atmos. 102, 3725–3735.
McGrath, M.J., Olenius, T., Ortega, I.K., Loukonen, V., Paasonen, P., Kurtén, T., et al., 2012. Atmospheric cluster dynamics code: a flexible method for solution of the birth-death equations. Atmo. Chem. Phys. 12, 2345–2355.
Meng, H., Zhu, Y.J., Evans, G.J., Jeong, C., Yao, X.H., 2015. Roles of SO_2 oxidation in new particle formation events. J. Environ. Sci. 30, 90–101.
Myllys, N., Elm, J., Halonen, R., Kurtén, T., Vehkamaki, H., 2016a. Coupled cluster evaluation of the stability of atmospheric acid-base clusters with up to 10 molecules. J. Phys. Chem. A 120, 621–630.
Myllys, N., Elm, J., Kurtén, T., 2016b. Density functional theory basis set convergence of sulfuric acid-containing molecular clusters. Comput. Theor. Chem. 1098, 1–12.
Neese, F., 2012. The ORCA program system. WIREs Comput. Mol. Sci. 2, 73–78.
Paasonen, P., Olenius, T., Kupiainen, O., Kurtén, T., Petäjä, T., Birmili, W., et al., 2012. On the formation of sulphuric acid-amine clusters in varying atmospheric conditions and its influence on atmospheric new particle formation. Atmo. Chem. Phys. 12, 9113–9133.
Qiao, K., Wu, Z.J., Pei, X.Y., Liu, Q.Y., Shang, D.J., Zheng, J., et al., 2018. Size-resolved effective density of submicron particles during summertime in the rural atmosphere of Beijing, China. J. Environ. Sci. 73, 69–77.
Ren, L.J., Bai, H.H., Yu, X., Wu, F.C., Yue, S.Y., Ren, H., et al., 2018. Molecular composition and seasonal variation of amino acids in urban aerosols from Beijing, China. Atmo. Res. 203, 28–35.
Řezáč, J., Fanfrlik, J., Salahub, D., Hobza, P., 2009. Semiempirical quantum chemical PM6 method augmented by dispersion and H-bonding correction terms reliably describes various types of noncovalent complexes. J. Chem. Theory Comput. 5, 1749–1760.
Riipinen, I., Sihto, S.L., Kulmala, M., Arnold, F., Dal Maso, M., Birmili, W., et al., 2007. Connections between atmospheric sulphuric acid and new particle formation during QUEST III-IV campaigns in Heidelberg and Hyyti. Atmo. Chem. Phys. 7, 1899–1914.
Riplinger, C., Neese, F., 2013. An efficient and near linear scaling pair natural orbital based local coupled cluster method. J. Chem. Phys. 138, 034106.
Saikia, J., Narzary, B., Roy, S., Bordoloi, M., Saikia, P., Saikia, B.K., 2016. Nanominerals, fullerene aggregates, and hazardous elements in coal and coal combustion-generated aerosols: An environmental and toxicological assessment. Chemosphere 164, 84–91.
Scalabrin, E., Zangrando, R., Barbaro, E., Kehrwald, N.M., Gabrieli, J., Barbante, C., et al., 2012. Amino acids in arctic aerosols. Atmo. Chem. Phys. 12, 10453–10463.

Schlesinger, W., Hartley, A., 1992. A global budget for atmospheric NH3. Biogeochemistry 15, 191–211.
Schobesberger, S., Junninen, H., Bianchi, F., Lönn, G., Ehn, M., Lehtipalo, K., et al., 2013. Molecular understanding of atmospheric particle formation from sulfuric acid and large oxidized organic molecules. Proc. Natl. Acad. Sci. USA 110, 17223–17228.
Shampine, L.F., Reichelt, M.W., 1997. The matlab ode suite. SIAM J. Sci. Comput. 18, 1–22.
Shi, X., Zhao, X.W., Zhang, R.M., Xu, F., Cheng, J.M., Zhang, Q.Z., et al., 2019. Theoretical study of the cis-pinonic acid and its atmospheric hydrolysate participation in the atmospheric nucleation. Sci. Total Environ. 674, 234–241.
Sipilä, M., Berndt, T., Petäjä, T., Brus, D., Vanhanen, J., Stratmann, F., et al., 2010. The role of sulfuric acid in atmospheric nucleation. Science 327, 1243–1246.
Steinfeld, J.I., 2006. Atmospheric chemistry and physics: from air pollution to climate change. John Wiley & Sons, Inc.
Stewart, J.J.P., 2013. Optimization of parameters for semiempirical methods VI: more modifications to the NDDO approximations and re-optimization of parameters. J. Mol. Model. 19, 1–32.
Vaittinen, O., Metsälä, M., Persijn, S., Vainio, M., Halonen, L., 2014. Adsorption of ammonia on treated stainless steel and polymer surfaces. Appl. Phys. B 115, 185–196.
Wang, C.Y., Ma, Y., Chen, J., Jiang, S., Liu, Y.R., Wen, H., et al., 2016. Bidirectional interaction of alanine with sulfuric acid in the presence of water and the atmospheric implication. J. Phys. Chem. A 120, 2357–2371.
Weber, R.J., Marti, J.J., Mcmurry, P.H., Eisele, F.L., Tanner, D.J., Jefferson, A., 2007. Measured atmospheric new particle formation rates: implications for nucleation mechanisms. Chem. Eng. Commun. 151, 53–64.
Xie, H.B., Elm, J., Halonen, R., Myllys, N., Kurtén, T., Kulmala, M., et al., 2017. Atmospheric fate of monoethanolamine: enhancing new particle formation of sulfuric acid as an important removal process. Environ. Sci. Technol. 51, 8422–8431.
Zhang, R.Y., 2010. Getting to the critical nucleus of aerosol formation. Science 328, 1366–1367.
Zhang, Q., Anastasio, C., 2003. Free and combined amino compounds in atmospheric fine particles (PM2.5) and fog waters from Northern California. Atmos. Environ. 37, 2247–2258.
Zhang, J., Dolg, M., 2016. Global optimization of clusters of rigid molecules using the artificial bee colony algorithm. Phys. Chem. Chem. Phys. 18, 3003–3010.
Zhang, Q., Anastasio, C., Jimenez-Cruz, M., 2002. Water-soluble organic nitrogen in atmospheric fine particles (PM2.5) from northern California. J. Geophys. Res.-Atmos. 107, 1–9.
Zhang, R.Y., Khalizov, A., Wang, L., Hu, M., Xu, W., 2012. Nucleation and growth of nanoparticles in the atmosphere. Chem. Rev. 112, 1957–2011.
Zhang, R.Y., Wang, G.H., Guo, S., Zamora, M.L., Ying, Q., Lin, Y., et al., 2015. Formation of urban fine particulate matter. Chem. Rev. 115, 3803–3855.
Zhang, H.J., Kupiainen-Määttä, O., Zhang, X.H., Molinero, V., Zhang, Y.H., Li, Z.S., 2017. The enhancement mechanism of glycolic acid on the formation of atmospheric sulfuric acid–ammonia molecular clusters. J. Chem. Phys. 146, 184308.
Zhang, H.J., Li, H., Liu, L., Zhang, Y.H., Zhang, X.H., Li, Z.S., 2018a. The potential role of malonic acid in the atmospheric sulfuric acid-ammonia clusters formation. Chemosphere 203, 26–33.
Zhang, R., Jiang, S., Liu, Y.R., Wen, H., Feng, Y.J., Huang, T., et al., 2018b. An investigation about the structures, thermodynamics and kinetics of the formic acid involved molecular clusters. Chem. Phys. 507, 44–50.
Zhao, Y., Truhlar, D.G., 2008. The M06 suite of density functionals for main group thermochemistry, thermochemical kinetics, noncovalent interactions, excited states, and transition elements: two new functionals and systematic testing of four M06-class functionals and 12 other functionals. Theor. Chem. Acc. 120, 215–241.